

Earth–Moon VLBI project. Modeling of scientific outcome

Sergei L. Kurdubov,¹[★] Dmitry A. Pavlov,¹ Svetlana M. Mironova,¹
and Sergey A. Kaplev²

¹ *Institute of Applied Astronomy of the Russian Academy of Sciences, Saint-Petersburg, Russia*

² *Federal State Unitary Enterprise “Central Research Institute for Machine Building”, Korolev, Russia*

Accepted XXX. Received YYY; in original form ZZZ

ABSTRACT

Modern radio astrometry has reached the limit of the resolution that is determined by the size of the Earth. The only way to overcome that limit is to create the radio telescopes outside our planet. It is proposed to build an autonomous remote-controlled radio observatory on the Moon. Working together with the existing radio telescopes on Earth in the VLBI mode, the new observatory will form an interferometer baseline up to 410 000 km, enhancing the present astrometric and geodetic capabilities of VLBI. We perform numerical simulations of Earth–Moon VLBI observations operating simultaneously with the international VLBI network. It is shown that these observations will significantly improve the precision of determination of Moon’s orbital motion, libration angles, ICRF, and relativistic parameters.

Key words: Moon – instrumentation: interferometer – ephemerides – reference systems – relativistic processes – methods: numerical

1 INTRODUCTION AND HISTORY

VLBI observations allow to determine various parameters important for astrometry or geodesy, such as coordinates of extragalactic radio sources, Earth rotation parameters, and coordinates of stations, with accuracy proportional to λ/b , where λ is the wavelength, and b is the baseline between two radio telescopes. At present, the wavelength is 7.5 mm or more, while the baseline is bounded by the diameter of the Earth. Expansion towards shorter wavelengths is hardened due to the atmospheric absorption, frequency standards instability and data acquisition system limitations. Hence the most straightforward way to improve the accuracy is the extension of the baseline outside Earth. Placing one of the interferometer antennae on the Moon will allow to increase the baseline by the factor of 60 for the international VLBI network.

The Moon serves as a platform for scientific experiment since Project Apollo. The most important experiments concerning lunar dynamics and selenodesy include: lunar laser ranging to five lunar retroreflectors (Apollo 11/14/15, Luna 17/21), the GRAIL experiment which measured the lunar gravitational field with unprecedented accuracy, and the Lunar Reconnaissance Orbiter (LRO) spacecraft that provides high-resolution mapping and altimetry. The lunar lander Chang’e 3, landed at the end of 2013, is operational to this day, as is LRO. It is evident that space agencies of different

countries are headed towards lunar exploration and maybe a habitable lunar baseline in near future. The far side of the Moon is of particular interest for astrophysical experiments because it is naturally shielded from Earth’s natural and artificial radio frequency interference (Douglas & Smith 1985; Lazio et al. 2009; Skalsky et al. 2014).

One of the earliest proposals of a Moon–Earth radio interferometry was made by Burns (1985, 1988). To this day, no attempt of such an experiment has been made; however, two orbital VLBI telescopes were built. The first, 8-meter HALCA (Hirabayashi et al. 2000), also known by its program name VSOP, provided VLBI observations from 1997 to 2003. The second, 10-meter RadioAstron (Kardashev et al. 2013), also known as Spectr-R, launched in 2011 and is still operational. However, while both HALCA and RadioAstron provided great observations for astrophysics, neither has been used for the purposes of astrometry. One reason for this is the difficulty of precise tracking the spacecraft orbit during the VLBI session, essential for building the reference frame but not so for obtaining images and studying the structure of the extragalactic radio sources.

One possible difficulty in VLBI on such a large baseline could be the loss of correlated flux densities. However, the Spectr-R results show that at least 160 quasars have very compact structures and high brightness temperatures, enough to obtain fringes at baselines up to 200 000 km (Kardashev et al. 2017).

Modern VGOS recording systems can register more than 100x wider bandwidth than Spectr-R formatter (16

[★] E-mail: kurdubov@iaaras.ru

MHz) and thus we can expect that the new instrument will have more than 10x sensitivity and that fringes will be obtained.

2 CONCEPT

2.1 Pros and cons of lunar environment

Placing a moving instrument on the lunar surface presents some great challenges, such as complicated landing and maintenance, temperature jumps, and solar radiation. On the other hand, in some sense the Moon provides better experimental conditions than Earth. Having no atmosphere and no oceans, the Moon has a much more stable rotational motion than the Earth; also, the absence of atmosphere eases the processing of observations and reduces errors that come from the ionosphere and troposphere interfering with observed radio noise. Low lunar gravity will allow lighter construction and machinery.

A spacecraft orbiting the Earth does not suffer from the atmosphere, too; however, the trajectory of a spacecraft is highly unstable as compared to an object tied to lunar surface. The biggest source of the instability is the solar pressure. It does affect the Moon, but its effect to the Moon is much more subtle, predictable, and stable (Vokrouhlický 1997). Furthermore the spacecraft orbit always will be a “byproduct” of astrometric observations whereas precise positioning of lunar based antenna gives significant contribution to selenodesy science.

In order to participate in modern astrometric and geodetic VLBI observations, an orbital VLBI telescope has to change targets fast. Modern Earth-based VGOS antennas have slewing speed up to 6 degree per second. Corresponding rotation of spacecraft in space can be achieved only with the reactive thrusters leading to a very unstable orbit. Also the fuel tanks will limit operational time.

2.2 Co-location

It is recommended that the new radio telescope is co-located with a retroreflector, either a panel of corner-cubes (Vasiliev et al. 2014), or a next generation single cube retroreflector (Turyshev et al. 2013; Araki et al. 2016). Requiring no power on the Moon and no data transmission, the Earth–Moon laser ranging would help to determine the precise location of the station, and also independently contribute to study of lunar dynamics, and building of the lunar reference frame, and testing general relativity (Murphy 2013; Williams et al. 2013b; Pavlov et al. 2016; Viswanathan et al. 2018).

Adding a GNSS receiver to the new lunar VLBI station will allow to receive signals from Earth satellites, when the Moon happens to be in the same beam with Earth when viewed from the satellite. Such observations would allow to improve the determination of orbits of the GNSS satellites in the celestial reference frame.

2.3 Choice of location

Only scientific outcome was considered as the primary criterion for location of the proposed station on the lunar surface.

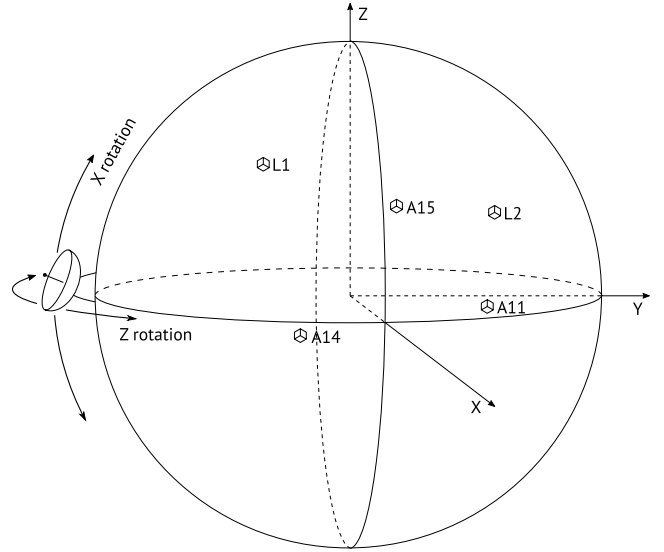


Figure 1. Five existing lunar retroreflector panels and the proposed VLBI station. The XY plane and the Z axis are close to lunar equator and rotation axis, respectively. The X axis is directed approximately towards the Earth.

Other criteria, such as: landing and deployment issues, local terrain, power supply, proximity to possible lunar baselines were not considered.

There are multiple reasons for the location to be chosen on the visible side of the lunar disc. First, it will allow direct Moon–Earth data transfer. Second, it will allow co-location with a lunar laser ranging (LLR) retroreflector and/or GNSS receiver (see Section 2.2). Third, it will allow a slight (roughly 9000 km) increase in the interferometry baseline, by observing the radio sources that are visible from the far (as viewed from the Moon) side of the Earth.

The location on the visible side of the Moon exposes the station to radio interference from the Earth (natural or artificial). However, the receiving pattern of the lunar radio telescope will be narrow, similarly to its Earth VLBI counterparts, so the radio interference will not be a problem.

Assuming only one instrument of this kind, it should be located close to the lunar equator so that the radio sources in both southern and northern hemispheres are visible.

The lunar laser ranging—currently the most precise tool to study the lunar physical librations—has low sensitivity to the rotation of the Moon around the Moon–Earth direction (see Fig. 1). The new VLBI station can achieve that sensitivity if it is placed outside the central area of the lunar disc. Another benefit of location outside the central area is that the new station extends the current lunar reference frame whose accuracy currently deteriorates outside the central area where are the five retroreflector points.

The chosen location in this work is on the visible part of the Moon’s equator, near its western end. The combination of the existing retroreflectors and the new VLBI instrument will allow to determine all three “instant” (daily/weekly/monthly) rotational corrections to the lunar orientation. LLR or VLBI alone are able to determine two rotations each.

3 DECISIONS ON THE LUNAR MODEL

3.1 Lunar dynamical model and ephemeris

We use the dynamical model of the orbital and rotational motion of the Moon implemented within the EPM planetary-lunar ephemeris (Pavlov et al. 2016). The rotational part of the model, involving tidal and rotational dissipation, as well as spherical liquid core, was proposed by Williams et al. (2001). Later improvements, such as core flattening and dedicated parameters describing influence of Earth’s tides to the orbit of the Moon, were implemented for DE430 ephemeris (Folkner et al. 2014). The third publicly available lunar ephemeris, INPOP, is presently based on the same model (Viswanathan et al. 2018).

Lunar ephemerides contain the geocentric (GCRF) position \mathbf{r} and velocity $\dot{\mathbf{r}}$ of the Moon as functions of time, and also the Euler angles ϕ , θ , and ψ and their rates as functions of time.

The lunar frame is aligned with the principal axes (PA) of the undistorted lunar mantle. The Euler angles define the matrix of the transformation from the lunar frame to the celestial frame:

$$R_{L2C}(t) = R_z(\phi(t))R_x(\theta(t))R_z(\psi(t)). \quad (1)$$

R_x and R_z are matrices of right-hand rotations of vectors around axes x and z , respectively. The argument t will be omitted when appropriate.

3.2 Daily lunar orientation parameters

We study the possibility of determination of daily corrections to the dynamical model of transformation from the lunar frame to the celestial frame.

$$R_{L2C}^{\text{daily}}(t) = R_x(\Delta X)R_y(\Delta Y)R_z(\Delta Z)R_{L2C}(t) \quad (2)$$

The daily corrections are assumed to be small and the order of the X , Y , Z rotations not relevant.

3.3 Determination of the reference point of the radio telescope

The VLBI technique requires precise determination of the position of the lunar radio telescope w.r.t. its Earth counterparts. Such a determination can be done in two different ways depending on the task:

(i) If the task is to build the lunar ephemeris and/or lunar reference frame, one should fit to observations the selenocentric position \mathbf{l}_{PA} of the lunar radio telescope. The VLBI reduction routine should use the determined \mathbf{l}_{PA} to obtain the GCRS position \mathbf{l}_{GCRS} :

$$\mathbf{l}_{GCRS}(t) = \mathbf{r}(t) + \mathbf{l}_{L2CRS}(t) \left(1 - \frac{U(t)}{c^2} \right) - \frac{\dot{\mathbf{r}}_B(t) \cdot \mathbf{l}_{L2CRS}(t)}{2c^2} \dot{\mathbf{r}}_B(t) \quad (3)$$

$$\mathbf{l}_{L2CRS}(t) = R_{L2C}(t) \mathbf{l}_{PA} + \Delta(\mathbf{l}_{PA}, t)$$

where U is the gravitational potential at the Moon’s center, excluding the Moon’s mass, \mathbf{r}_B and $\dot{\mathbf{r}}_B$ are the barycentric

position and velocity of the Moon, and Δ is the displacement due to solid Moon tide raised by Earth and Sun.

(ii) For the purposes of astrometry, it is more natural to determine geocentric, rather than selenocentric, position of the lunar radio telescope. That will give justification to fix and not to determine the lunar ephemeris together with the whole Earth–Moon VLBI solution. The link between the lunar ephemeris and the geocentric position of the retroreflector is relatively small.

The VLBI reduction should then use the determined $\mathbf{l}_{GCRS}(t_0)$ to solve for $\mathbf{l}_{L2CRS}(t_0)$, then solve for \mathbf{l}_{PA} , and finally calculate $\mathbf{l}_{GCRS}(t)$ by equation (3).

To estimate the accuracy of determination of $\mathbf{l}_{GCRS}(t_0)$, the relativistic and tidal terms can be neglected and the derivative matrix of $\mathbf{l}_{GCRS}(t)$ w.r.t. $\mathbf{l}_{GCRS}(t_0)$ will be simplified to

$$\frac{d\mathbf{l}_{GCRS}(t)}{d\mathbf{l}_{GCRS}(t_0)} \approx R_{L2C}(t)R_{L2C}^T(t_0) \quad (4)$$

4 SETTING OF EXPERIMENT

4.1 Data

We simulated two-week intensive Earth–Moon VLBI campaign similar to a subset of CONT17 (ivscc.gsfc.nasa.gov/program/cont17). The “Legacy-1” subset was taken; it has 14 VLBI stations in Europe, Russia, South Africa, Australia, New Zealand, Brazil, Japan, and Hawaii. To each scan of Earth radio telescopes observing a source, we add a set of Earth–Moon VLBI delays of the same source for each of the Earth radio telescopes participating in the session. Scans involving a quasar not visible from the lunar radio telescope at the specified time were excluded. The final dataset contains 24 095 Earth–Moon simulated VLBI delays and 105 808 real delays on Earth–Earth baselines for nine days. The whole campaign lasted 15 days (November 28 – December 12, 2017), but observations from the remaining six days of the “Legacy-1” subset were not available at the time of writing.

Of the three CONT17 subsets—“Legacy-1”, “Legacy-2”, and “VGOS-Demo”—the first one has the best expected accuracy on the EOP determination. For comparison, we also took the “Legacy-2” subset in the simulation of the determination of lunar orientation parameters and PPN parameter γ (see sections 4.5 and 5.4). 36 589 Earth–Moon delays were generated and used for that subset.

Simulations of Earth–Moon VLBI delays for different subsets were done separately, not simultaneously, due to the time overlap.

For one part of the experiment (see Section 4.3), we used the real LLR data spanning from 1970 to the end of 2017. The most important observations at present are performed at Apache Point Observatory (Murphy et al. 2012; Murphy 2013) and Observatoire de la Côte d’Azur (Samain et al. 1998; Courde et al. 2017). More information about re-weighting and reductions of LLR observations is given in (Pavlov et al. 2016). Some observations were considered erroneous and were filtered out. Most often the observations from the McDonald Laser Ranging Station (1988–2015) did not fit well into the model. Of total 25 535 LLR observations, 773 were filtered out and 24 762 were used in the lunar solution.

4.2 Software

Two independent software packages were used. ERA-8 (Pavlov & Skripnichenko 2015) was used to fit the parameters of the lunar model to observations, and to integrate lunar ephemeris (Section 4.3). An extension was made to ERA-8 to process Earth–Moon VLBI delays (in addition to LLR normal points) as part of a global lunar solution. QUASAR (Gubanov & Kurdubov 2014) was used to obtain the VLBI solution for celestial reference frame, using a fixed lunar ephemeris. An extension was made to QUASAR to bring a VLBI station to the Moon, determine its location in Section 4.4 or the lunar orientation parameters in Section 4.5.

4.3 Estimating the improvement of the lunar ephemeris

Two estimations of the accuracy of the lunar ephemeris were obtained: the first using real LLR observations (1970–2017), and the second using LLR and 15 days of simulated VLBI observations in the end of 2017.

The celestial and terrestrial VLBI frames were fixed. The formal error of the simulated Earth–VLBI observations was set to 7 mm (1σ), similarly to the postfit RMS discrepancy of the ionosphere-free combination for global VLBI solution.

Each of the determined parameters falls into one of the two categories:

(i) Dynamical parameters: initial Euler angles of lunar physical libration and their rates; initial GCRS position and velocity of the Moon; initial core angular velocity; undistorted J_2 , C_{32} , S_{32} , S_{33} of the Moon; ratios between undistorted main moments of inertia of the Moon; lunar core flattening and friction coefficient; two Earth tidal delays; GM of the Earth–Moon system.

(ii) Reduction parameters: positions and velocities of LLR stations; selenocentric (PA) positions of the lunar retroreflectors; Love number h_2 of the Moon; 28 specific biases for different time intervals. The selenocentric lunar radio telescope position was determined as well in the solution with 15 days of simulated VLBI observations.

The details about the determined parameters are given in (Pavlov et al. 2016), however, for this work, two changes were made. One of them is the aforementioned determination of J_2 . Not fixing J_2 to a GRAIL-determined value brings more realistic uncertainties into the lunar solution. The second change is that the additional three kinematic terms of the longitude libration (with amplitudes in several mas) were not determined and thus absorbed into other dynamical parameters’ formal errors.

Parameters from both categories were determined simultaneously using the least-squares method, their formal errors and covariance matrix were calculated.

In addition to the dynamical parameters, the dynamical model also has constant undistorted Stokes coefficients of Earth’s gravitational potential (up to degree 6) taken from EGM2008 (Pavlis et al. 2012) solution, and Moon’s gravitational potential (C_{30} , C_{31} , S_{31} , and others of degrees 4–6) from GL1200 (Goossens et al. 2016) solution. From the latter solution, the lunar k_2 Love number is also used.

The covariance matrix of the parameters under variation was formed as a submatrix of the lunar solution covariance matrix with excluded reduction parameters, to which rows and columns were added corresponding to the constants. The resulting matrix \mathbf{M} had size $(n + k) \times (n + k)$, where $n = 28$ was the number of the dynamical determined parameters and $k = 83$ was the number of constants.

In the added rows and columns, squares of the formal errors of corresponding constants were assigned to the diagonal terms, while the off-diagonal terms were set to zero.

The Monte-Carlo simulation of the lunar ephemeris was done in the following way. The Cholesky decomposition of the covariance matrix was calculated: $\mathbf{M} = \mathbf{L}^T \mathbf{L}$, where \mathbf{L} is a lower triangular matrix. Each sample X for the simulation was obtained as a sample from the multidimensional normal distribution described by \mathbf{M} : $X = \mathbf{L}^T Y$, where Y is a $(n + k)$ -vector sample of independent normally distributed random variables with zero mean and unit variance.

For each of the sampled X , a corresponding ephemeris of orbital and rotational motion of the Moon was obtained by numerical integration. The integrated dynamical model contained not only the Moon, but also the Sun, all planets, Pluto, Ceres, Pallas, Vesta, Iris, and Bamberga. The parameters related to non-lunar part of the model were not varied, because their influence on the lunar ephemeris is relatively small, and their influence on the lunar ephemeris uncertainty is negligibly small.

The chosen epoch was January 2, 2018, and numerical integration was for five years forward (2018–2022). The scatter of the determined initial parameters of the Moon (position and Euler angles) and the evolution of those parameters over time was studied. Two different Monte-Carlo simulations were done, one with only LLR observations, and the other with LLR and simulated VLBI observations. 1000 samples were generated for each of the two simulations.

4.4 Estimating the improvement of the celestial reference frames

In order to estimate the accuracy of celestial reference frame we perform the solution over all CONT17 data with source right ascension and declinations as global parameters. The tropospheric delay, clock synchronisation parameters, LOP and EOP were estimated for each session.

For the Earth baselines we also use the model noise instead of real VLBI observations because the real VLBI data depends heavily on clock corrections and the procedure of determination of those corrections should work with consistent O-C values. Since do not have Earth–Moon VLBI data consistent with real Earth VLBI clock, we took the correlator estimated noise for all observations. The noise was multiplied by the factor of 4, which is an ad-hoc value that represents the clock, troposphere etc. scatter from real world and was found from comparison of parameter errors obtained in Earth VLBI processing with model noise and real VLBI data.

4.5 Estimating the determination of the lunar orientation parameters

LOP estimation was done in a similar manner to the celestial reference frame determination (sec. 4.4).

Table 1. Uncertainty of the selenocentric reference points in two solutions. A = Apollo, L = Lunokhod, LRT = lunar radio telescope

Coordinate	3σ (LLR only)	3σ (LLR and VLBI)
A11 X	14.5 cm	0.5 cm
A11 Y	19.4 cm	2.0 cm
A11 Z	5.3 cm	1.4 cm
L1 X	15.7 cm	0.5 cm
L1 Y	13.9 cm	2.3 cm
L1 Z	8.5 cm	4.8 cm
A14 X	12.8 cm	0.5 cm
A14 Y	19.9 cm	2.0 cm
A14 Z	5.4 cm	1.4 cm
A15 X	11.5 cm	0.4 cm
A15 Y	18.8 cm	1.6 cm
A15 Z	7.9 cm	3.5 cm
L2 X	14.0 cm	0.4 cm
L2 Y	16.5 cm	2.2 cm
L2 Z	7.5 cm	3.5 cm
LRT X	N/A	1.5 mm
LRT Y	N/A	0.9 mm
LRT Z	N/A	0.6 mm

With the chosen location of the lunar radio telescope (Section 2.3), its position in the celestial reference frame will be sensitive to ΔX and ΔZ daily corrections but not to ΔY .

The ΔX and ΔZ corrections were assumed independent and constant for each of the nine days of the “Legacy-1” subset of the CONT17 campaign with simulated Earth–Moon VLBI data.

For comparison, similar simulation was done with the “Legacy-2” subset spanning 15 consecutive days.

Lunar laser ranging can also independently contribute to determination of the lunar orientation parameters. However, Earth–Moon ranges are sensitive to Y and Z rotations but have almost no sensitivity to X rotations. As shown by Pavlov & Yagudina (2017), the formal errors of daily (nightly) ΔY and ΔZ obtained on real LLR data are 1–2 mas at best.

5 RESULTS OF PARAMETER ESTIMATION

5.1 Lunar ephemeris, lunar reference frame, and Moon–Earth reference frame

Positions of lunar reference points were determined simultaneously with parameters of orbit and physical libration of the Moon, and other parameters (see Section 4.3).

Table 1 shows the accuracy of the lunar reference frame implemented by five retroreflector points (in case of real LLR data) or five retroreflector plus one radio telescope point (with real LLR and simulated VLBI data). One can see a 6x–10x improvement in accuracy of the existing five points from the VLBI data. One of the key factors of such a major improvement is that the VLBI observations are “omnidirectional”, i.e. they measure the projections of the “Earth observatory – Lunar radio telescope” vector to all directions, and so they are sensitive to the orbital position of the Moon. LLR observations are sensitive to the Earth–Moon distance but not much to the position of the Moon on orbit.

Table 2. Uncertainty of the geocentric (at epoch 02.01.2018) reference points in two solutions. A = Apollo, L = Lunokhod, LRT = lunar radio telescope

Coordinate	3σ (LLR only)	3σ (LLR and VLBI)
A11 X	3.9 cm	2.0 cm
A11 Y	2.9 cm	0.9 cm
A11 Z	14.0 cm	1.3 cm
L1 X	3.1 cm	2.2 cm
L1 Y	3.5 cm	1.7 cm
L1 Z	14.1 cm	4.4 cm
A14 X	3.1 cm	1.9 cm
A14 Y	3.2 cm	1.1 cm
A14 Z	14.4 cm	1.4 cm
A15 X	2.6 cm	1.4 cm
A15 Y	3.8 cm	1.7 cm
A15 Z	13.6 cm	3.2 cm
L2 X	3.7 cm	2.2 cm
L2 Y	3.2 cm	1.4 cm
L2 Z	13.7 cm	3.2 cm
LRT X	N/A	0.9 mm
LRT Y	N/A	1.7 mm
LRT Z	N/A	1.0 mm

Table 2 is similar to Table 1 but it shows the accuracy in the geocentric at epoch (see Section 3.3). In the LLR-only solution, the geocentric positions of retroreflector are determined ≈ 1.6 x better than the selenocentric ones. It is known that the X coordinate of each lunar retroreflector panel strongly correlates with the GM of the Earth–Moon system and also with the semimajor axis of the Moon at the epoch (see e.g. Williams et al. 2013a). The correlation causes the selenocentric position of a retroreflector at epoch and the position of the Moon at epoch to be detected with less accuracy than the geocentric position of the retroreflector at epoch.

As for the “LLR+VLBI” solution, the geocentric and selenocentric positions of the six lunar points are determined with similar accuracy overall, thanks again to the VLBI measuring in all directions.

To estimate the accuracy of either lunar or Moon–Earth reference frame not at epoch, but for some time into the future, one can look at Figs. 2 and 3. Maximum and root-mean-square deviations of sampled ephemeris (see Section 4.3) w.r.t. the nominal ephemeris are plotted. In five years without new observations, the accuracy of the Moon’s orbital position determined via 47 years or LLR degrades to 4.6 m (maximum); when LLR is combined with nine days of Earth–Moon VLBI observations, the maximum error drops to 0.6 m. Similarly, the 5-year maximum error of lunar physical libration is 1.3 m with LLR and 0.15 m with LLR+VLBI.

5.2 Lunar orientation parameters

The formal errors of the daily ΔX and ΔZ detected from Earth–Moon VLBI simulations are shown at Figs. 4 (“Legacy-1” subset of CONT17) and 5 (“Legacy-2”). It can be seen that both rotations are determined with uncertainty (3x the formal error) 0.3 mas or lower with “Legacy-1”. With the other subset, the uncertainties are ≈ 1.5 x bigger, despite the larger number of observations than in the first subset.

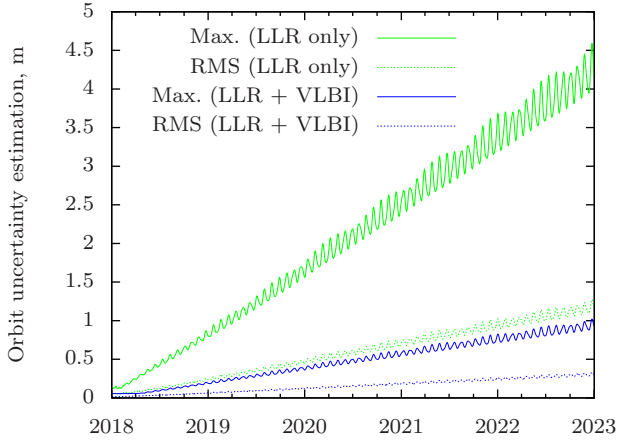


Figure 2. Estimation (maximum and RMS) of the uncertainty of the orbital position of the Moon for five years, assuming no observations since 2018, using only LLR data or LLR data with simulated VLBI data

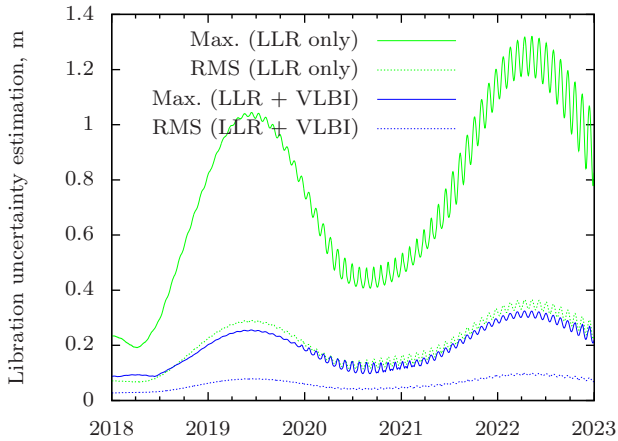


Figure 3. Estimation (maximum and RMS) of the uncertainty of the lunar physical libration (measured in maximum discrepancy across the lunar surface) for five years, assuming no observations since 2018, using only LLR data or LLR data and simulated VLBI data

This comparison agrees with the original CONT17 estimations for the EOP determination.

5.3 Celestial reference frame

In order to show the impact of lunar VLBI observation on improvement of celestial reference frame realization we estimate radio source positions using only CONT17 Earth based observations and observations with Earth–Moon baselines. Results are presented on Figs. 6 and 7 for right ascension and declination, respectively. The plots show formal errors of source positions for Earth and Earth–Moon observations. One can see that for moderate number of sources one Moon-based telescope improves positions accuracy by more than ten times.

The formal errors for the best sources of the ICRF are

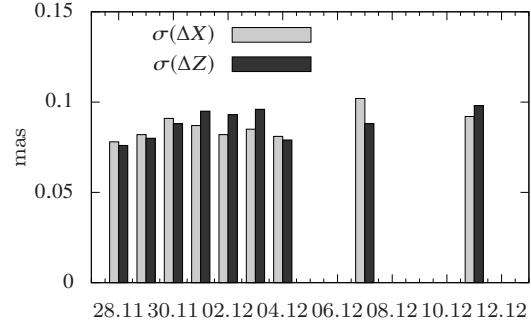


Figure 4. Formal errors (1σ) of determined lunar orientation parameters (X and Z rotations) in “CONT17 Legacy-1 with lunar radio telescope” scenario

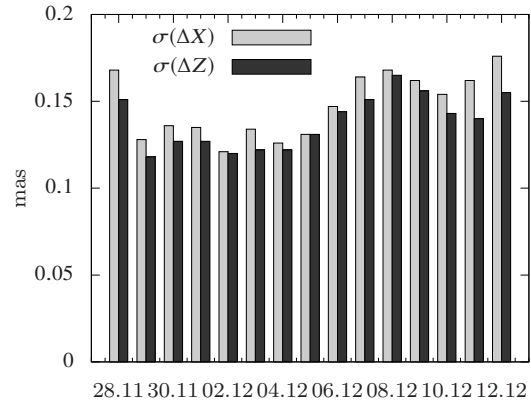


Figure 5. Formal errors (1σ) of determined lunar orientation parameters (X and Z rotations) in “CONT17 Legacy-2 with lunar radio telescope” scenario

about tens of microarcseconds (Fey et al. 2015), which is smaller than the “Earth-only” results on Figs. 6 and 7. That is because our estimates are based on nine days’ data, while the ICRF is built using the results from 40 years of VLBI observations. The Earth–Moon VLBI results, also estimated from nine days of observations, will improve with longer timespan.

Fig. 8 shows the ratio of the formal errors of determined declinations without Earth–Moon VLBI to those with Earth–Moon VLBI, relative to ecliptic latitude. The ratio were multiplied by square root of number of observations with Earth–Moon VLBI divided by number of observations without Earth–Moon VLBI. One can see that points on Fig. 8 are greater than 1 for all latitudes and more than 10 for about half of the sources. The improvement are the least for latitudes close to zero because the Earth–Moon baseline and source unit vectors are both close to the ecliptic plane.

Interstellar scattering and intrinsic source structure effects may limit position errors obtained by Earth–Moon VLBI to greater than those shown in Figs. 6 and 7. However, the Earth–Moon VLBI can help to estimate the source structure, in the manner similar to present VLBI observations (see e.g. Frey et al. 2018). There are techniques in de-

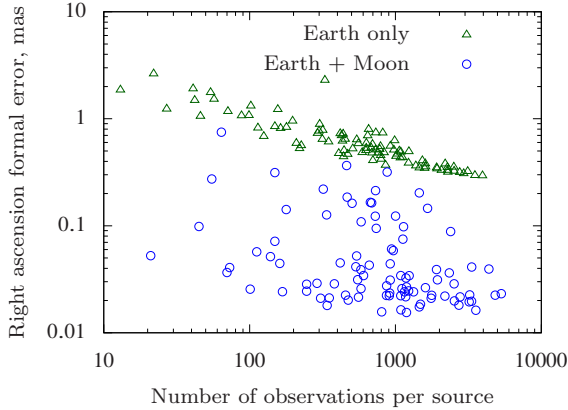


Figure 6. Formal errors (1σ) of determined right ascensions of observed radio sources from CONT “Legacy-1” observations, with and without Earth–Moon VLBI

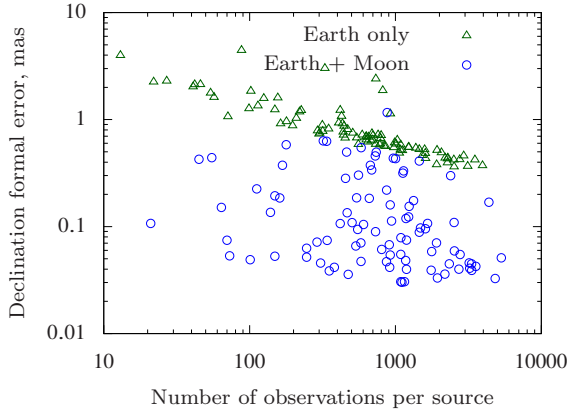


Figure 7. Formal errors (1σ) of determined declinations of observed radio sources from CONT “Legacy-1” observations, with and without Earth–Moon VLBI

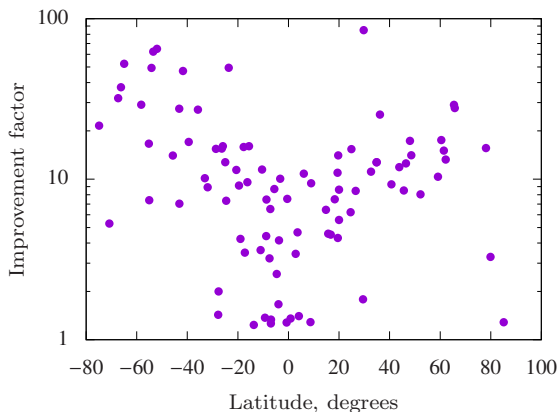


Figure 8. Improvement factor (Earth and Earth–Moon VLBI vs just Earth VLBI) of radio source declination formal error normalized by square root of relative number of observations (as a function of ecliptic latitude).

Table 3. Delay generated by gravity of a body (Δt_G) and by its translational motion (Δt_M)

Body	Baseline, km	Angle	Δt_G	Δt_M
Sun	6000	grazing ray	169.24 ns	0.0082 ps
Sun	6000	1 deg	45.33 ns	
Sun	6000	30 deg	1.47 ns	
Sun	6000	90 deg	0.40 ns	
Sun	6000	175 deg	17.25 ps	
Sun	380000	grazing ray	8588.24 ns	0.4166 ps
Sun	380000	1 deg	3098.72 ns	
Sun	380000	30 deg	93.59 ns	
Sun	380000	90 deg	25.02 ns	
Sun	380000	175 deg	1.11 ns	

velopment to apply the source structure map to astrometric VLBI delay calculation.

5.4 General relativity tests

Relativistic contribution by Solar system bodies to VLBI time delay arises with baseline b . Using the equation from (Klioner 1991), we computed the gravitational delay and delay due to translational motion for baselines $b = 6000$ km and $b = 380000$ km. Table 3 shows the delays for different baseline lengths (the second column) different angles between source unit vector and baseline vector (the third column). It is visible that delay generated by the Sun is detectable for two antennas located on Earth only if the angle is less than 30 degrees. Locating one of the antennas on the Moon will make that delay detectable on all angles.

The model of VLBI time delay contains PPN parameter γ which characterize space curvature produced by unit rest mass. The accuracy of γ estimated by initial CONT17 “Legacy-1” VLBI series $2.0 \cdot 10^{-3}$ has been obtained, while the estimation from “Legacy-1” and “Legacy-2” gives $1.3 \cdot 10^{-3}$. Adding Earth–Moon VLBI improves the accuracy to $0.5 \cdot 10^{-3}$ for “Legacy 1” and to $0.06 \cdot 10^{-3}$ for “Legacy-1” and “Legacy-2”.

The experiment was not specially designed for estimation of γ and does not have sources close to the Sun or Jupiter. Nevertheless, we obtain improvement factor from 4 to 21. A dedicated experiment like (Titov et al. 2018) with Earth–Moon VLBI can overcome the presently best accuracy $0.23 \cdot 10^{-4}$ obtained from frequency shift measurements of Cassini spacecraft (Bertotti et al. 2003).

Epstein & Shapiro (1980) also show that post-post-Newtonian deflection of the Sun is about $11 \mu\text{arcsec}$ which corresponds to delay equal to 1.1 ps for $b = 6000$ km and 67.6 ps for $b = 380000$ km. Therefore growth of the baseline will increase the accuracy of relativistic effects detection.

6 CIRCULUNAR ORBIT DETERMINATION SIMULATION

A dedicated numerical simulation was performed to study the impact of lunar reference frame improvement (Table 1) to the determination of orbits of an example lunar satellite constellation. Nine satellites were modeled with circular inclined orbits with semimajor axis of 4500 km. The model ob-

Table 4. Range accuracy of orbit determination example based on ISL and two-way range measurements to the reference points with different uncertainties

Reference points by:	LLR only	LLR and VLBI
RMS (3.5 h measurements)	7.9 cm	2.7 cm
95% CI (3.5 h measurements)	12.9 cm	4.8 cm
Max. (3.5 h measurements)	16.2 cm	8.0 cm
RMS (12 h propagation)	14.8 cm	7.8 cm
95% CI (12 h propagation)	26.5 cm	14.5 cm
Max. (12 h propagation)	43.3 cm	24.4 cm

servations were: inter-satellite links (ISL) measurements and two-way range measurements to the retroreflector points.

Table 4 shows the accuracy of given constellation orbit determination projected to the average lunar surface point line-of-sight for two scenarios of reference points uncertainties according to Table 1 columns. ISL measurement accuracies were assumed to be at a few centimeter level (1σ) to make the results sensitive to the differences between the reference points uncertainties. Solution is produced with the least squares method using the measurement interval of 3.5 hours equals to about the half of orbital period and the following propagation interval of 12 hours. Statistics was taken over all satellites in the constellation. Three values are provided for each time interval: root-mean-square value, maximum value over 95% confidence interval, and maximum value overall.

The results show a $\approx 2x$ improvement in orbit determination accuracy after suggested Earth–Moon VLBI implementation.

7 CONCLUSION

For the purposes of astrometry, the placement of the lunar radio telescope near equator, close to the edge of the visible side of the lunar disc is preferred.

The obtained results are based on the assumption that the sensitivity of the proposed Earth–Moon interferometer will be enough for obtaining accurate time delay (i. e. the existence of sufficiently bright and compact quasar structures is assumed).

Just nine days of intensive Earth–Moon VLBI observations will improve the accuracy of the Earth–Moon reference frame $3x$ – $6x$, and the accuracy of the lunar reference frame $4x$ – $10x$. The accuracy of the lunar ephemeris (both orbit and physical libration), presently calculated from 47 years of LRR, will improve from meters to decimeters for five-year interval into the future.

The accuracy of daily corrections to lunar orientation reach 0.3 mas (≈ 2.5 mm on the lunar surface) for X and Z rotations. With the chosen location of the instrument, Y rotations can not be determined from Earth–Moon VLBI; however, LLR is capable of determining them, while with accuracy of 3 – 5 mas (centimeters on the lunar surface).

According to simulated observations for nine days, the accuracy of the celestial reference frame can be improved more than $10x$ for about half of the radio sources distant from ecliptic. The Earth–Moon interferometer will have higher sensitivity to the relativistic parameters of post-

Newtonian and post-post-Newtonian formalism and can be used for relativistic tests.

The lunar reference frame, improved by the Earth–Moon VLBI, will bring a $\approx 2x$ improvement in accuracy of the determination of orbits of a possible lunar satellite constellation. However, such an improvement, while important for fundamental lunar science, will not be critical for applications like lunar navigation with the present requirements.

Some of the results promised by Earth–Moon VLBI relevant to study of the Moon itself could in principle be accomplished with other tools (more precise LLR, lunar radio transponders, lunar optical telescope), while orbital radio telescopes are useful for astrophysics. However, the Earth–Moon VLBI will stand unrivaled for future radio astrometry and building of the Earth–Moon reference frame.

ACKNOWLEDGEMENTS

Authors from the IAA RAS are thankful to Iskander Gayazov, Alexander Ipatov, Dmitry Vavilov, and numerous other colleagues for helpful discussion, advice, and support throughout this work.

The current state of lunar study, used in this work as a starting point, would not have been possible without the effort of personnel at observatories doing lunar laser ranging. Similarly, the VLBI data used in this work was a result of a many-year effort of different people and organizations from different countries. Particularly, the Continuous VLBI Campaign managed by the IVS provides an inspiring insight of capabilities of international collaboration.

REFERENCES

- Araki H., et al., 2016, *Earth, Planets and Space*, 68, 101
 Bertotti B., Iess L., Tortora P., 2003, *Nature*, 425, 374
 Burns J. O., 1985, in Mendell W. W., ed., *Lunar Bases and Space Activities of the 21st Century*. pp 293–300, <http://adsabs.harvard.edu/abs/1985lbsa.conf..293B>
 Burns J. O., 1988, in NASA Conference Publication. pp 97–104, <https://ntrs.nasa.gov/archive/nasa/casi.ntrs.nasa.gov/19890006452>
 Courde C., et al., 2017, *A&A*, 602, A90
 Douglas J. N., Smith H. J., 1985, in Mendell W. W., ed., *Lunar Bases and Space Activities of the 21st Century*. pp 301–306, <http://adsabs.harvard.edu/abs/1985lbsa.conf..301D>
 Epstein R., Shapiro I. I., 1980, *Phys. Rev. D*, 22, 2947
 Fey A. L., et al., 2015, *The Astronomical Journal*, 150, 58
 Folkner W., Williams J., Boggs D., Park R., Kuchynka P., 2014, IPN Progress Report 42-196, *The Planetary and Lunar Ephemerides DE430 and DE431*. NASA JPL, http://naif.jpl.nasa.gov/pub/naif/generic_kernels/spk/planets/de430.bsp
 Frey S., Titov O., Melnikov A. E., de Vicente P., Shu, F. 2018, *A&A*, 618, A68
 Goossens S. J., et al., 2016, in *Lunar and Planetary Science Conference XLVII*. <https://www.hou.usra.edu/meetings/lpsc2016/pdf/1484.pdf>
 Gubanov V. S., Kurdubov S. L., 2014, in Behrend D., Baver K. D., Armstrong K. L., eds, *International VLBI Service for Geodesy and Astrometry 2014 General Meeting Proceedings: “VGOS: The New VLBI Network”*. Science Press, Beijing, China, pp 325–329, http://ivscc.gsfc.nasa.gov/publications/gm2014/070_Gubanov_Kurdubov.pdf
 Hirabayashi H., et al., 2000, *Publications of the Astronomical Society of Japan*, 42, 955

- Kardashev N. S., et al., 2013, *Astronomy Reports*, 57, 153
- Kardashev N. S., et al., 2017, *Solar System Research*, 51, 535
- Klioner S. A., 1991, in *Geodetic VLBI: Monitoring Global Change*. p. 188, <http://adsabs.harvard.edu/abs/1991gvmg.conf..188K>
- Lazio J., Carilli C., Hewitt J., Furlanetto S., Burns J., 2009, *Proc.SPIE*, 7436
- Murphy T. W., 2013, *Reports on Progress in Physics*, 76, 076901
- Murphy T., Adelberger E., Battat J., Hoyle C., Johnson N., McMillan R., Stubbs C., Swanson H., 2012, *Class. Quantum Grav.*, 29, 184005
- Pavlis N. K., Holmes S. A., Kenyon S. C., Factor J. K., 2012, *Journal of Geophysical Research: Solid Earth*, 117
- Pavlov D., Skripnichenko V., 2015, in Malkin Z., Capitaine N., eds, *Proceedings of the Journées 2014 “Systèmes de référence spatio-temporels”*. Pulkovo Observatory, pp 243–246, <http://synte.obspm.fr/jsr/journees2014/pdf/Pavlov.pdf>
- Pavlov D. A., Yagudina E. I., 2017, *Transactions of IAA RAS*, 43, 104
- Pavlov D. A., Williams J. G., Suvorkin V. V., 2016, *Celestial Mechanics and Dynamical Astronomy*, 126, 61
- Samain E., et al., 1998, *Astron. Astrophys. Suppl. Ser.*, 130, 235
- Skalsky A., Zelenyi L., Rothkaehl H., Gurvits L., Sadovskiy A., Mogilevsky M., Gotlib V., 2014, in 40th COSPAR Scientific Assembly. <http://adsabs.harvard.edu/abs/2014cosp...40E..61S>
- Titov O., et al., 2018, *A&A*, 618, A8
- Turyshev S. G., et al., 2013, *Experimental Astronomy*, 36, 105
- Vasiliev V. P., Sadovnikov M. A., Sokolov A. L., Shargorodski V. D., 2014, in 19h International Workshop on Laser Ranging. <https://cddis.nasa.gov/lw19/docs/2014/Abstracts/3024.pdf>
- Viswanathan V., Fienga A., Minazzoli O., Bernus L., Laskar J., Gastineau M., 2018, *Monthly Notices of the Royal Astronomical Society*, 476, 1877
- Vokrouhlický D., 1997, *Icarus*, 126, 293
- Williams J. G., Boggs D. H., Yoder C. F., Ratcliff J. T., Dickey J. O., 2001, *Journal of Geophysical Research: Planets*, 106, 27933
- Williams J. G., Boggs D. H., Folkner W. M., 2013a, Jet Propulsion Laboratory Interoffice Memorandum 335-JW,DB,WF-20130722-016, DE430 Lunar Orbit, Physical Librations, and Surface Coordinates. California Institute of Technology, http://naif.jpl.nasa.gov/pub/naif/generic_kernels/spk/planets/de430_moon_coord.pdf
- Williams J. G., Boggs D. H., Ratcliff J. T., 2013b, in *Lunar and Planetary Science Conference*. p. 2377, <https://www.lpi.usra.edu/meetings/lpsc2013/pdf/2377.pdf>

This paper has been typeset from a \LaTeX file prepared by the author.